BUCKLING ANALYSIS OF FUNCTIONALLY GRADED SANDWICH PLATES RESTING ON PASTERNAK FOUNDATION USING A NOVEL REFINED QUASI-3D THIRD-ORDER SHEAR DEFORMATION THEORY

Vu Tan Van[a,*], Nguyen Van Hieu[a]

[a]*Department of Civil Engineering, University of Architecture Ho Chi Minh City, Ho Chi Minh City, 196 Pasteur street, Ward Vo Thi Sau, District 3, Ho Chi Minh City, Vietnam*

Abstract

This study presents a numerical model for buckling analysis of the functionally graded sandwich plates (FGSP) laid on the elastic foundation through the Moving Kriging interpolation-based meshless method using a refined quasi-3D third-order shear deformation theory. The in-plane displacements encompassed a new third-order polynomial in terms of the thickness coordinate, will satisfy the natural vanishing of transverse shear stresses on the top and bottom surfaces. Furthermore, the displacement fields approximated by only four variables with accounting for the thickness stretching effect can lead to the reduction of computational time. Comparison investigations are studied to justify the accuracy of the present method. The influence of the aspect ratios, gradient index, and elastic foundation parameters on the normalized buckling load of FGSP is also studied and discussed.

Keywords: functionally graded plates; third-order shear deformation theory; Moving Kriging interpolation-based method; Pasternak's foundation.

1. Introduction

The sandwich-structured composite consists of two or more homogeneous elastic layers combined together to form a high-performance material. This feature made it widely applied in many engineering branches. Nevertheless, the unexpected change in material properties among the layers may cause through-thickness failure because of interlaminar stresses. To overcome this drawback, the functionally graded materials (FGM) with continuously mechanical varying properties for layers are used. Nowadays, the model of FGM plates laid on elastic supports has been widely employed for many engineering problems. It is well-known that the 2-dimensional shear deformation theories (2DSDTs) including the classical plate theory [1] (CPT), first-order shear deformation theory [2] (FSDT), third-order shear deformation theory [3] (TSDT), higher-order shear deformation theory [4] (HSDT) and refined plate theory [5] (RPT) can be employed for the FGM plate analysis. Because the transverse displacement is assumed constant across the plate thickness, these 2DSDTs ignore the influence of thickness extending (i.e., $\varepsilon_{zz} = 0$.) on numerical models. Carrera et al. [6] reported that the

---

Corresponding author. E-mail address: van.vutan@uah.edu.vn (Van, V. T.)

effect of thickness extending can not be ignored for the moderately thick FGM plates. Consequently, many researchers suggested quasi-3-dimensional shear deformation theories (Q-3DSDT) based on Murakami's zigzag-shaped function [7] (MZF) or Carrera's unified formulation (CUF) [8] for studying the mechanical behaviour of the plates with considering the thickness stretching. However, the MZF-based and CUF-based theories are complex and costly since they utilize an enormous amount of displacement unknowns, e.g. Carrera et al. [9] employed 15 displacement unknowns, Talha and Singh [10], Ganapathi and Makhecha [11] employed 13 displacement unknowns, Chen at al. [12] and Reddy [13] employed 11 displacement variables, Ferreira et al. [14–16] and Neves et al. [17–19] employed 9 unknowns in the displacement field. Recently, Zenkour [20] presents a simple quasi-3D shear deformation theory (SQ-3DSDT) wherein the displacement field is approximated by only four variables as the same case of the CPT, but accounting for the thickness stretching. Furthermore, one of the main conveniences of the SQ-3DSDT is that it has shear locking free for thin plates and fewer variables than those of the FSDT and HSDT. Nevertheless, the SQ-3DSDT needs the shape function based on the displacement field must be at least C^1 continuous, as the result, it obstructs the natural use of the conventional finite element method (FEM) which possessed the C^0 continuity. To overcome this obstacle, one of the solutions is to use meshless method (MM) in which its shape functions could be easily established for any orders of continuity.

According to the formulation procedure, MM can be classified into three groups including weak forms, strong forms, and weak–strong forms. Among the weak-form-based approaches, a well-known MM using the moving Kriging interpolation-based (MKI) [21] with the shape function having the Kronecker delta property possessed the boundary conditions enforced explicitly as for the FEM without using any special techniques. Unfortunately, the correlation parameter had a significant impact on the quality of traditional MKI shape functions, resulting in unstable solutions. Van et al. [22, 23] has recently attempted to overcome this limitation by improving the quality of the MK shape function through the key improvement in order to get rid of the correlation parameter effect. Utilizing this enhanced MKI-based meshfree method [22], Van et al. [24] analyzed the static bending and free vibration problems of functionally graded porous plates laid on elastic foundation based on the refined quasi-3D sinusoidal shear deformation theory.

In this work, for the first time, the buckling analysis of FGSP resting on the elastic Pasternak foundations by a new refined quasi-3D third-order shear deformation theory (RQ-3DTSDT) integrated with MKI-based meshfree method based on the quadric correlation function [23] is presented.

2. Theoretical formulations

A considered rectangular FGSP with the thickness h and the width a and depth b is shown in Fig. 1(a). It consists of three homogeneous or FGM layers having the same Poisson's ratio υ laying on Pasternak's foundation. The effective Young's modulus $E_{eff}(z)$ of FGM layers can be determined by using the power-law distribution defined by Eq. (1)

$$E_{eff}(z) = E_m + (E_c - E_m) V_c(z) \qquad (1)$$

where E_c and E_m are the Young's moduli of the ceramic and metal constituents, respectively; $V_c(z) = (0.5 + z/h)^\beta$ with β is the gradient index, respectively.

2.1. FGSP with homogeneous core and FGM skins (Type-A)

The FGSP type-A consists of a homogeneous core and two skins whose metal-rich at surfaces $z = z_1, z = z_4$ and ceramic-rich at surfaces $z = z_2, z = z_3$, is shown in Fig. 1(b). The volume fraction

of the P-FGM skins can be computed by Eqs. (2), (3), and (4)

$$V_c^{(1)}(z) = \left(\frac{z - z_1}{z_2 - z_1}\right)^\beta, \quad z \in [z_1, z_2] \tag{2}$$

$$V_c^{(2)}(z) = 1, \qquad z \in [z_2, z_3] \tag{3}$$

$$V_c^{(3)}(z) = \left(\frac{z_4 - z}{z_4 - z_3}\right)^\beta, \quad z \in [z_3, z_4] \tag{4}$$

where $(z_2 - z_1)$ and $(z_4 - z_3)$ are thicknesses of bottom and top skins. The thickness index of each plate layer $(z_4 - z_3)/(z_3 - z_2)/(z_2 - z_1)$ is defined as the various ratios 2/1/2; 2/2/1 and so on.

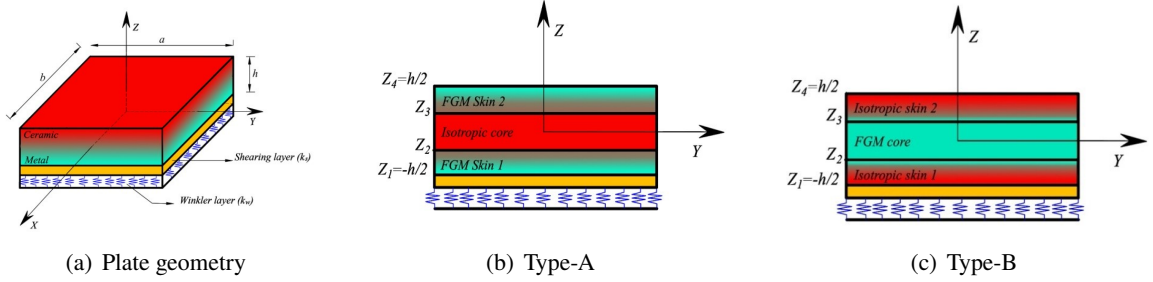(a) Plate geometry   (b) Type-A   (c) Type-B

Figure 1. The sandwich FG plate

2.2. FGSP with FGM core and homogeneous skins (Type-B)

Fig. 1(c) depicts the FGSP type-B consisting of a P-FGM core and two homogeneous layers. The volume fraction of this FG sandwich can be found in Eqs. (5), (6), and (7)

$$V_c^{(1)}(z) = 0, \quad z \in [z_1, z_2] \tag{5}$$

$$V_c^{(2)}(z) = \left(\frac{z - z_2}{z_3 - z_2}\right)^\beta, \quad z \in [z_2, z_3] \tag{6}$$

$$V_c^{(3)}(z) = 1, \quad z \in [z_3, z_4] \tag{7}$$

where $V_c^{(i)}, (i = 1, 2, 3)$ is volume fraction function of layer i; $(z_3 - z_2)$ is core thickness.

2.3. An proposed RQ-3DTSDT integrated with the MKI element-free Galerkin method

Let Ω be a domain $\mathbb{R}^2$ located in the mid-plane of the plate. Regarding the tension effect in z direction, the plate displacements u, v and w in the x, y and z directions, respectively can be modeled with only four displacement variables [20] as follows:

$$u(x, y, z) = u_0(x, y) - z\frac{\partial w_{0,1}(x, y)}{\partial x} + f(z)\frac{\partial w_{0,2}(x, y)}{\partial x} \tag{8}$$

$$v(x, y, z) = v_0(x, y) - z\frac{\partial w_{0,1}(x, y)}{\partial y} + f(z)\frac{\partial w_{0,2}(x, y)}{\partial y} \tag{9}$$

$$w(x, y, z) = w_{0,1}(x, y) + w_{0,2}(x, y)g(z) \tag{10}$$

in which $u_0(x, y), v_0(x, y)$ and $w_{0,1}(x, y)$ are the displacements of the middle plane ($z = 0$) in the x, y, z direction, while $w_{0,2}(x, y)$ is the additional displacement that considered an effect of normal stress.

New transverse shear deformation functions that satisfying naturally the vanished condition at the outer surfaces of the plate for transverse shear stresses are chosen as $f(z) = 7z/4 - 7z^3/3h^2$ and $g(z) = 7/12 - 7z^2/3h^2$, respectively. The functions $f(z)$ and $g(z)$, which represent the realistic parabolic distribution of transverse shear strains and stresses across the plate thickness, are carefully chosen to satisfy the traction-free boundary conditions and obtained through numerical comparisons of the obtained results with available analytical solutions. The strain-displacement relations are given by Eqs. (11) and (12)

$$\bar{\varepsilon} = \left\{ \begin{matrix} \varepsilon_{xx} & \varepsilon_{yy} & \gamma_{xy} & \varepsilon_{zz} \end{matrix} \right\}^T = \bar{\varepsilon}_0 + z\bar{\varepsilon}_1 + f(z)\bar{\varepsilon}_2 + g'(z)\bar{\varepsilon}_3 \tag{11}$$

$$\bar{\gamma} = \left\{ \begin{matrix} \gamma_{xz} & \gamma_{yz} \end{matrix} \right\}^T = [f'(z) + g(z)]\bar{\varepsilon}_s \tag{12}$$

wherein $\bar{\varepsilon}_s = \left\{ \dfrac{\partial w_{0,2}}{\partial x} \quad \dfrac{\partial w_{0,2}}{\partial y} \right\}^T$, $\bar{\varepsilon}_0 = \left\{ \dfrac{\partial u_0}{\partial x} \quad \dfrac{\partial v_0}{\partial y} \quad \dfrac{\partial u_0}{\partial y} + \dfrac{\partial v_0}{\partial x} \quad 0 \right\}^T$, $\bar{\varepsilon}_1 = -\left\{ \dfrac{\partial^2 w_{0,1}}{\partial x^2} \quad \dfrac{\partial^2 w_{0,1}}{\partial y^2} \right.$

$\left. 2\dfrac{\partial^2 w_{0,1}}{\partial x \partial y} \quad 0 \right\}^T$, $\bar{\varepsilon}_2 = \left\{ \dfrac{\partial^2 w_{0,2}}{\partial x^2} \quad \dfrac{\partial^2 w_{0,2}}{\partial y^2} \quad 2\dfrac{\partial^2 w_{0,2}}{\partial x \partial y} \quad 0 \right\}^T$, $\bar{\varepsilon}_3 = \left\{ 0 \quad 0 \quad 0 \quad w_s \right\}^T$ while $f'(z) = \dfrac{\partial f(z)}{\partial z}$,

$g'(z) = \dfrac{\partial g(z)}{\partial z}$ and are the first derivatives with respect to z, respectively. The stress-strain behaviour can be formed in general Hooke's law as

$$\left\{ \begin{matrix} \sigma_{xx} \\ \sigma_{yy} \\ \sigma_{zz} \\ \tau_{yz} \\ \tau_{xz} \\ \tau_{xy} \end{matrix} \right\} = \left\{ \begin{matrix} Q_{11}(z) & Q_{12}(z) & Q_{13}(z) & 0 & 0 & 0 \\ Q_{12}(z) & Q_{22}(z) & Q_{23}(z) & 0 & 0 & 0 \\ Q_{13}(z) & Q_{23}(z) & Q_{33}(z) & 0 & 0 & 0 \\ 0 & 0 & 0 & Q_{44}(z) & 0 & 0 \\ 0 & 0 & 0 & 0 & Q_{55}(z) & 0 \\ 0 & 0 & 0 & 0 & 0 & Q_{66}(z) \end{matrix} \right\} \left\{ \begin{matrix} \varepsilon_{xx} \\ \varepsilon_{yy} \\ \varepsilon_{zz} \\ \varepsilon_{yz} \\ \varepsilon_{xz} \\ \varepsilon_{xy} \end{matrix} \right\} \tag{13}$$

where $\sigma = \left\{ \begin{matrix} \sigma_{xx} & \sigma_{yy} & \sigma_{zz} & \tau_{yz} & \tau_{xz} & \tau_{xy} \end{matrix} \right\}^T$ and $\varepsilon = \left\{ \begin{matrix} \varepsilon_{xx} & \varepsilon_{yy} & \varepsilon_{zz} & \varepsilon_{yz} & \varepsilon_{xz} & \varepsilon_{xy} \end{matrix} \right\}^T$ are stress tensor and strain tensor, respectively. The elastic coefficients $Q_{ij}(z)$ can be given below:

$$Q_{11}(z) = Q_{22}(z) = Q_{33}(z) = \frac{E_{eff}(z)(1 - \upsilon)}{(1 - 2\upsilon)(1 + \upsilon)} \tag{14}$$

$$Q_{12}(z) = Q_{13}(z) = Q_{23}(z) = \frac{E_{eff}(z)\upsilon}{(1 - 2\upsilon)(1 + \upsilon)} \tag{15}$$

$$Q_{44}(z) = Q_{55}(z) = Q_{66}(z) = \frac{E_{eff}(z)}{2(1 + \upsilon)} \tag{16}$$

Considering an FG plate with two-parameter elastic foundation, the total potential energy can be written as below:

$$\Xi = \frac{1}{2} \int_V \left[\sigma_{xx}\varepsilon_{xx} + \sigma_{yy}\varepsilon_{yy} + \sigma_{zz}\varepsilon_{zz} + \tau_{xz}\gamma_{xz} + \tau_{yz}\gamma_{yz} + \tau_{xy}\gamma_{xy} \right] dV + \dots$$

$$\dots + \frac{1}{2} \int_\Theta \left\{ k_w w^2 + k_s \left[\left(\frac{\partial w}{\partial x} \right)^2 + \left(\frac{\partial w}{\partial y} \right)^2 \right] + F_x^0 \frac{\partial^2 w}{\partial x^2} + F_y^0 \frac{\partial^2 w}{\partial y^2} + 2F_{xy}^0 \frac{\partial^2 w}{\partial x \partial y} \right\} d\Theta \tag{17}$$

where k_w and k_s are the Winkler's stiffness and shear stiffness coefficients of the elastic foundation, respectively; F_x^0, F_y^0 and F_{xy}^0 are the in-plane compressive forces per unit length.

2.4. Meshless formulation for buckling analysis of the FG plates rested on the elastic foundations

Let us consider a distribution function $u(\mathbf{x}_i)$ that was approximated in the sub-domain $\wp_x$ ($\wp_x \subseteq \Theta$) over a number of n scattered nodes $\mathbf{x}_1, \mathbf{x}_2, ..., \mathbf{x}_n$. The MK interpolation function $u^h(\mathbf{x})$, $\forall \mathbf{x} \in \wp_x$ can be expressed as follows:

$$u^h(\mathbf{x}) = \left[\breve{\mathbf{p}}^T(\mathbf{x})\bar{\breve{\mathbf{A}}} + \breve{\mathbf{r}}^T(\mathbf{x})\bar{\breve{\mathbf{B}}} \right] \mathbf{u}(\mathbf{x}) \tag{18}$$

or

$$u^h(\mathbf{x}) = \sum_{I=1}^{n} N_i(\mathbf{x})\mathbf{u}_I \tag{19}$$

in which the MK shape function $N_i(\mathbf{x})$ is set by

$$N_i(\mathbf{x}) = \sum_{j=1}^{m} \breve{p}_j(\mathbf{x})\breve{A}_{jI} + \sum_{k=1}^{n} \breve{r}_k(\mathbf{x})\breve{B}_{kI} \tag{20}$$

with

$$\bar{\breve{\mathbf{A}}} = \left(\bar{\breve{\mathbf{P}}}^T \bar{\breve{\mathbf{R}}}^{-1} \bar{\breve{\mathbf{P}}} \right)^{-1} \bar{\breve{\mathbf{P}}}^T \bar{\breve{\mathbf{R}}}^{-1} \tag{21}$$

$$\bar{\breve{\mathbf{B}}} = \bar{\breve{\mathbf{R}}}^{-1} \left(\bar{\breve{\mathbf{I}}} - \bar{\breve{\mathbf{P}}}\bar{\breve{\mathbf{A}}} \right) \tag{22}$$

Matrix $\bar{\breve{\mathbf{I}}}$ denotes an identity matrix, and in Eq. (18) $\breve{\mathbf{p}}^T(\mathbf{x})$ and $\breve{\mathbf{r}}^T(\mathbf{x})$ are defined by:

$$\breve{\mathbf{p}}^T(\mathbf{x}) = [\breve{p}_1(\mathbf{x}), \breve{p}_2(\mathbf{x}), \ldots, \breve{p}_m(\mathbf{x})] \tag{23}$$

$$\breve{\mathbf{r}}^T(\mathbf{x}) = [R(\mathbf{x}_1, \mathbf{x}), R(\mathbf{x}_2, \mathbf{x}), \ldots, R(\mathbf{x}_n, \mathbf{x})] \tag{24}$$

In Eq. (21) matrix $\bar{\breve{\mathbf{P}}}_{n\times m}$ comprised values of the vital functions determined by Eq. (25) while $\bar{\breve{\mathbf{R}}}\left[R\left(\mathbf{x}_i, \mathbf{x}_j\right)\right]_{n\times n}$ included the so-called correlation matrix determined by Eq. (26) at the given nodes, they are shown as below:

$$\bar{\breve{\mathbf{P}}}_{n\times m} = \begin{bmatrix} \breve{p}_1(\mathbf{x}_1) & \breve{p}_2(\mathbf{x}_1) & \cdots & \breve{p}_m(\mathbf{x}_1) \\ \breve{p}_1(\mathbf{x}_2) & \breve{p}_2(\mathbf{x}_2) & \cdots & \breve{p}_m(\mathbf{x}_2) \\ \vdots & \vdots & \ddots & \vdots \\ \breve{p}_1(\mathbf{x}_n) & \breve{p}_2(\mathbf{x}_n) & \cdots & \breve{p}_m(\mathbf{x}_n) \end{bmatrix} \tag{25}$$

$$\bar{\breve{\mathbf{R}}}\left[R\left(\mathbf{x}_i, \mathbf{x}_j\right)\right] = \begin{bmatrix} 1 & R(\mathbf{x}_1, \mathbf{x}_2) & \cdots & R(\mathbf{x}_1, \mathbf{x}_n) \\ R(\mathbf{x}_2, \mathbf{x}_1) & 1 & \cdots & R(\mathbf{x}_2, \mathbf{x}_n) \\ \vdots & \vdots & \ddots & \vdots \\ R(\mathbf{x}_n, \mathbf{x}_1) & R(\mathbf{x}_n, \mathbf{x}_2) & \cdots & 1 \end{bmatrix} \tag{26}$$

In order to enhance the quality of the conventional MKI shape function, we use the quadric correlation function [23] $R(\mathbf{x}_i, \mathbf{x}_j) = \left(1 - r_{ij}/l_{\mathbf{x}}\sqrt{2}\right)^2$. Also, $l_{\mathbf{x}}$ denotes the mean distance between the given nodes $\mathbf{x}_i$ ($i = 1, ..., n$) within the support domain. The influence domain was determined by $d_m = \alpha d_c$, wherein d_c is a characteristic length, and α denotes a scaling factor.

2.5. Discrete governing equations

Generalized displacements of the FG plate in Eqs. (8), (9), and (10) can be approximated in terms of the displacements at nodes

$$\tilde{\mathbf{w}}^h = \begin{bmatrix} \tilde{w}_{0,1}^h & \tilde{w}_{0,2}^h & \tilde{w}_{0,3}^h & \tilde{w}_{0,4}^h \end{bmatrix}^T \quad \text{and} \quad \tilde{\mathbf{w}}_I = \begin{bmatrix} \tilde{w}_{0,1I} & \tilde{w}_{0,2I} & \tilde{w}_{0,3I} & \tilde{w}_{0,4I} \end{bmatrix}^T \tag{27}$$

Substitute Eq. (19) into Eqs. (11) and (12), we obtain the strain expressions after some algebraic manipulations:

$$\bar{\bar{\boldsymbol{\varepsilon}}}_1 = \sum_{I=1}^{n} \bar{\bar{\mathbf{B}}}_I^{b1} \tilde{\mathbf{w}}_I \tag{28}$$

$$\bar{\bar{\boldsymbol{\varepsilon}}}_2 = \sum_{I=1}^{n} \bar{\bar{\mathbf{B}}}_I^{b2} \tilde{\mathbf{w}}_I \tag{29}$$

$$\bar{\bar{\boldsymbol{\varepsilon}}}_3 = \sum_{I=1}^{n} \bar{\bar{\mathbf{B}}}_I^{b3} \tilde{\mathbf{w}}_I \tag{30}$$

$$\bar{\bar{\boldsymbol{\varepsilon}}}_4 = \sum_{I=1}^{n} \bar{\bar{\mathbf{B}}}_I^{b4} \tilde{\mathbf{w}}_I \tag{31}$$

$$\bar{\bar{\boldsymbol{\varepsilon}}}_5 = \sum_{I=1}^{n} \bar{\bar{\mathbf{B}}}_I^{b5} \tilde{\mathbf{w}}_I \tag{32}$$

where $\bar{\bar{\mathbf{B}}}_I^{b1}, \bar{\bar{\mathbf{B}}}_I^{b2}, \bar{\bar{\mathbf{B}}}_I^{b3}, \bar{\bar{\mathbf{B}}}_I^{b4}$ and $\bar{\bar{\mathbf{B}}}_I^{b5}$ are given by

$$\bar{\bar{\mathbf{B}}}_I^{b1} = \begin{bmatrix} N_{I,x} & 0 & 0 & 0 \\ 0 & N_{I,y} & 0 & 0 \\ N_{I,y} & N_{I,x} & 0 & 0 \\ 0 & 0 & 0 & 0 \end{bmatrix} \tag{33}$$

$$\bar{\bar{\mathbf{B}}}_I^{b2} = \begin{bmatrix} 0 & 0 & -N_{I,xx} & 0 \\ 0 & 0 & -N_{I,yy} & 0 \\ 0 & 0 & -2N_{I,xy} & 0 \\ 0 & 0 & 0 & 0 \end{bmatrix} \tag{34}$$

$$\bar{\bar{\mathbf{B}}}_I^{b3} = \begin{bmatrix} 0 & 0 & 0 & N_{I,xx} \\ 0 & 0 & 0 & N_{I,yy} \\ 0 & 0 & 0 & 2N_{I,xy} \\ 0 & 0 & 0 & 0 \end{bmatrix} \tag{35}$$

$$\bar{\bar{\mathbf{B}}}_I^{b4} = \begin{bmatrix} 0 & 0 & 0 & 0 \\ 0 & 0 & 0 & 0 \\ 0 & 0 & 0 & 0 \\ 0 & 0 & 0 & N_I \end{bmatrix} \tag{36}$$

$$\bar{\bar{\mathbf{B}}}_I^{b5} = \begin{bmatrix} 0 & 0 & 0 & N_{I,x} \\ 0 & 0 & 0 & N_{I,y} \end{bmatrix} \tag{37}$$

Using Eqs. (13), (17) and applying a weak formulation [25], the discretized equations for the buckling analysis of the FG plate can be obtained by solving the eigenvalue problem: $\left(\mathbf{K}_\Delta - \lambda_{cr} \mathbf{K}_{\Delta g} \right) \bar{\mathbf{u}} = \mathbf{0}$ in which $\mathbf{K}$ denoting the global stiffness can be determined by

$$
\mathbf{K}_\Delta = \int_V
\begin{Bmatrix}
\bar{\bar{\mathbf{B}}}_I^{b1} \\
\bar{\bar{\mathbf{B}}}_I^{b2} \\
\bar{\bar{\mathbf{B}}}_I^{b3} \\
\bar{\bar{\mathbf{B}}}_I^{b4}
\end{Bmatrix}^T
\begin{bmatrix}
\mathbf{T}^{d1} & \mathbf{T}^{d2} & \mathbf{T}^{d4} & \mathbf{T}^{d5} \\
\mathbf{T}^{d2} & \mathbf{T}^{d3} & \mathbf{T}^{d6} & \mathbf{T}^{d7} \\
\mathbf{T}^{d4} & \mathbf{T}^{d6} & \mathbf{T}^{d8} & \mathbf{T}^{d9} \\
\mathbf{T}^{d5} & \mathbf{T}^{d7} & \mathbf{T}^{d9} & \mathbf{T}^{d10}
\end{bmatrix}
\begin{Bmatrix}
\bar{\bar{\mathbf{B}}}_I^{b1} \\
\bar{\bar{\mathbf{B}}}_I^{b2} \\
\bar{\bar{\mathbf{B}}}_I^{b3} \\
\bar{\bar{\mathbf{B}}}_I^{b4}
\end{Bmatrix}
dV + \int_V \left(\bar{\bar{\mathbf{B}}}_I^{b5} \right)^T \mathbf{D}_s \bar{\bar{\mathbf{B}}}_I^{b5} dV
$$

$$
+ \int_\Theta \mathbf{N}_I^T k_w \mathbf{N}_I d\Theta + \int_\Theta k_s \left[\left(\bar{\bar{\mathbf{B}}}_I^{g1} \right)^T \bar{\bar{\mathbf{B}}}_I^{g1} + \left(\bar{\bar{\mathbf{B}}}_I^{g2} \right)^T \bar{\mathbf{B}}_I^{g2} \right] d\Theta
\tag{38}
$$

wherein

$$
\left\{ T_{ij}^{d1}, T_{ij}^{d2}, T_{ij}^{d3}, T_{ij}^{d4}, T_{ij}^{d5} \right\} = \int_{-h/2}^{h/2} \left\{ 1, z, z^2, f(z), g'(z) \right\} \bar{\bar{Q}}_{ij}(z) \, dz
\tag{39}
$$

$$
D_{ij}^s = \int_{-h/2}^{h/2} [f'(z) + g(z)]^2 \bar{\bar{G}}_{ij}(z) \, dz
\tag{40}
$$

$$
\left\{ T_{ij}^{d6}, T_{ij}^{d7}, T_{ij}^{d8}, T_{ij}^{d9}, T_{ij}^{d10} \right\} = \int_{-h/2}^{h/2} \left\{ zf(z), zg'(z), f^2(z), f(z)g'(z), g'^2(z) \right\} \bar{\bar{Q}}_{ij}(z) \, dz
\tag{41}
$$

Matrices $\bar{\bar{\mathbf{Q}}}(z)$ and $\bar{\bar{\mathbf{G}}}(z)$ express the material constitutive behaviors

$$
\bar{\bar{\mathbf{Q}}}(z) =
\begin{bmatrix}
Q_{11}(z) & Q_{12}(z) & 0 & Q_{13}(z) \\
Q_{12}(z) & Q_{22}(z) & 0 & Q_{23}(z) \\
0 & 0 & Q_{44}(z) & 0 \\
Q_{13}(z) & Q_{23}(z) & 0 & Q_{33}(z)
\end{bmatrix}
\tag{42}
$$

$$
\bar{\bar{\mathbf{G}}}(z) =
\begin{bmatrix}
Q_{55}(z) & 0 \\
0 & Q_{66}(z)
\end{bmatrix}
\tag{43}
$$

The global geometric stiffness matrix $\mathbf{K}_{\Delta g}$ is expressed as follows

$$
\mathbf{K}_{\Delta g} = \int_\Theta \left(\bar{\bar{\mathbf{B}}}_I^{g1} \right)^T
\begin{bmatrix}
F_x^0 & F_{xy}^0 \\
F_{xy}^0 & F_y^0
\end{bmatrix}
\bar{\bar{\mathbf{B}}}_I^{g1} d\Theta + \int_\Theta \left(\bar{\bar{\mathbf{B}}}_I^{g2} \right)^T
\begin{bmatrix}
\hat{F}_x^0 & \hat{F}_{xy}^0 \\
\hat{F}_{xy}^0 & \hat{F}_y^0
\end{bmatrix}
\bar{\bar{\mathbf{B}}}_I^{g2} d\Theta
\tag{44}
$$

where $\bar{\bar{\mathbf{B}}}_I^{g1} = \begin{bmatrix} 0 & 0 & N_{I,x} & 0 \\ 0 & 0 & N_{I,y} & 0 \end{bmatrix}$, $\bar{\bar{\mathbf{B}}}_I^{g2} = \begin{bmatrix} 0 & 0 & 0 & N_{I,x} \\ 0 & 0 & 0 & N_{I,y} \end{bmatrix}$, $\left\{ \hat{F}_x^0, \hat{F}_y^0, \hat{F}_{xy}^0 \right\} = \int_{-h/2}^{h/2} \left\{ F_x^0, F_y^0, F_{xy}^0 \right\} g^2(z) dz$.

A second-order polynomial basis $\breve{p}^T(\hat{\mathbf{x}}) = \left\{ 1 \quad x \quad y \quad x^2 \quad xy \quad y^2 \right\}$ employed in Eq. (25). Furthermore, the quadratic polynomial basic function ($m = 6$) and the mesh with (4×4) Gauss points are employed to constructing the MK shape function.

3. Numerical results

3.1. Numerical validations

This section deals with the accuracy of the proposed method for predicting the normalized buckling load of FGSP plates rested on the elastic foundation. The FGSP plate boundaries are noted by the following symbols: (F) signifies a totally free border; (S) indicates a simply supported border; and (C) pertains to a fully clamped border. First, we calculate the normalized buckling load of the square plate Al/ZnO$_2$ Type-A using the boundary conditions SSSS with a thickness-to-length ratio $a/h = 10$ and Poisson's ratio $\nu = 0.3$. In this study, material properties of Metal (Aluminum, Al): $E_m = 70 \times 10^9$ N/mm^2 and of Ceramic (Zirconia, ZrO$_2$): $E_c = 151 \times 10^9$ N/mm^2. In all examples, the foundation parameters are expressed in non-dimensional forms as $K_w^c = k_w a^4/D_c$, $K_s^c = k_s a^2/D_c$ with $D_c = E_c h^3/12(1 - \nu^2)$. Table 1 shows the comparison of normalized buckling loads for the FGSP plates rested on two-parameter elastic foundation calculated by the present method and expressed in the normalized form of $N_{cr} = \lambda_{cr} a^2/100h^3$ for several gradient indices under uni-axial and bi-axial

Table 1. Normalized buckling load N_{cr} of the simply-supported square plate ($a/h = 10$) Type-A Al/ZnO$_2$ for the uni-axial and bi-axial compression

Schemes	β	Methods	Uni-axial compression (K_w^c, K_s^c)			Bi-axial compression (K_w^c, K_s^c)		
			0, 0	10, 10	100, 100	0, 0	10, 10	100, 100
2-1-2	0.0	Akavci [26]	5.1127	7.9382	33.3348	2.5563	3.9691	16.6674
		Present	5.2723	8.1788	34.3170	2.6365	4.0902	17.1734
	2.0	Akavci [26]	2.8455	5.6690	31.0244	1.4227	2.8345	15.5122
		Present	2.9113	5.8178	32.1766	1.4558	2.9095	15.9928
	10.0	Akavci [26]	2.4809	5.3040	30.6456	1.2404	2.6520	15.3228
		Present	2.5379	5.4443	31.5965	1.2691	2.7228	15.8060
1-1-1	2.0	Akavci [26]	3.0116	5.8353	31.1957	1.5058	2.9177	15.5978
		Present	3.0814	5.9879	32.0738	1.5408	2.9946	16.0778
	10.0	Akavci [26]	2.6004	5.4235	30.7689	1.3002	2.7118	15.3845
		Present	2.6593	5.5658	31.7486	1.3298	2.7835	15.8668
2-2-1	2.0	Akavci [26]	3.1761	6.0002	31.3670	1.5881	3.0001	15.6835
		Present	3.2511	6.1576	32.2629	1.6257	3.0794	16.1627
	10.0	Akavci [26]	2.7764	5.6002	30.9562	1.3882	2.8001	15.4781
		Present	2.8395	5.7460	31.5850	1.4199	2.8736	15.9569
1-2-1	2.0	Akavci [26]	3.3125	6.1367	31.5059	1.6563	3.0683	15.7529
		Present	3.3911	6.2977	32.4128	1.6957	3.1494	16.2327
	10.0	Akavci [26]	2.8790	5.7025	31.0592	1.4395	2.8513	15.5296
		Present	2.9447	5.8512	31.9025	1.4725	2.9262	16.0095

compression with those reported by Akavci [26]. It is noteworthy that results obtained by the present method are in good accuracy for all schemes of the FGSP. Furthermore, the normalized buckling loads increase with decrease of the gradient index and strongly depend on the foundation stiffness parameters.

3.2. Parametric studies

Investigations were carried out for the analysis of normalized buckling loads for the simply-supported edges Al/ZnO$_2$ Type-B (a/h = 10) under the bi-axial compression. Table 2 shows the values of the normalized buckling loads of the plate using various schemes with respect to gradient indices. The normalized stiffness coefficients of the Pasternak foundation are given as K_w^c = 10 and K_s^c = 100. It can be observed from the table results that the increase of the gradient indices will lead to the decrease of the normalized buckling loads. In the case of the gradient indices less than unity, the normalized buckling loads increase with increasing in the core layer thickness, however, with decreasing the skin layer thickness. Meanwhile, the normalized buckling loads decrease with increase in the core layer thickness and with decreasing of the skin layer thickness in case of the gradient indices greater than 2.

Table 2. Influence of gradient index on the normalized buckling load N_{cr} for square SSSS plate a/h = 10 Type-B Al/ZnO$_2$ with elastic foundation (K_w^c = 10, K_s^c = 100)

| Schemes	Gradient index β							
	0.0	0.5	1.0	2.0	5.0	6.0	8.0	10
1-1-1	15.7176	15.6698	15.6512	15.6375	15.6291	15.6282	15.6270	15.6263
1-3-1	15.8976	15.7351	15.6739	15.6310	15.6024	15.5983	15.5919	15.5872
1-5-1	16.0209	15.7780	15.6867	15.6224	15.5762	15.5687	15.5569	15.5479
0-1-0	16.4829	15.9317	15.7233	15.5723	15.4420	15.4166	15.3753	15.3431
3-1-3	15.6592	15.6475	15.6424	15.6381	15.6349	15.6345	15.6341	15.6338
5-1-5	15.6504	15.6441	15.6412	15.6386	15.6365	15.6362	15.6359	15.6357

In Fig. 2, the effect of the length-to-thickness ratio a/h on the normalized buckling loads of the plate rested the Pasternak foundation (K_w^c = 10, K_s^c = 10) is displayed. It can be seen in this figure that increasing the ratio of a/h leads to an increase in the normalized buckling loads for the case of thick and moderately thick plates ($a/h \leq 50$).

Also, the plate (0-1-0) giving the smallest normalized buckling loads for the case of homogeneous metallic (β = 10) and the maximum values of those with the homogeneous ceramic (β = 0). Furthermore, the effect of width-to-length ratio b/a on the normalized buckling loads for the plate using two configurations of (1-8-1) and (8-1-8) is shown in Fig. 3. As shown in this figure the effect of the shear stiffness coefficient is more effective than Winkler's spring stiffness coefficient when increasing the plate normalized buckling loads. It can be concluded that increasing the ratio of b/a leads to increase in the normalized buckling loads.

Finally, the influence of the boundary conditions on the normalized buckling loads for the plate using the scheme of (1-1-1) is given in Table 3. It is observed that, for all cases the normalized buckling load decreases with the increasing of the gradient index but at different rates depending on whether the plate boundary condition is simply supported, clamped or clamped – simply supported. It is noticeable from Table 2 that the normalized buckling load N_{cr} increases with higher restraining
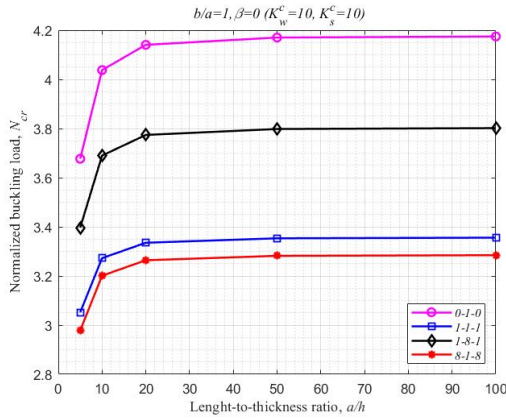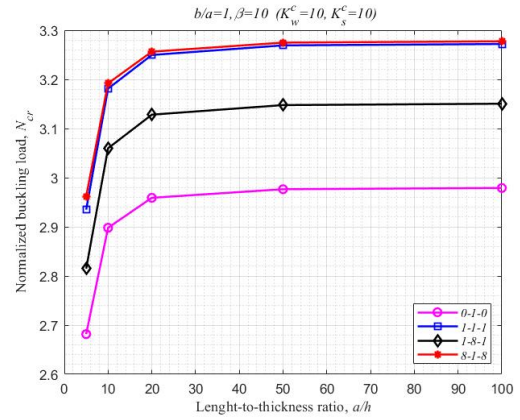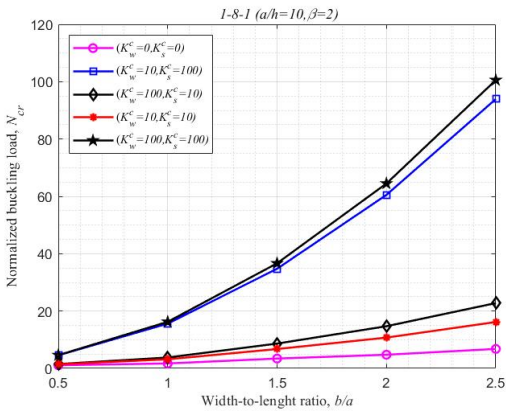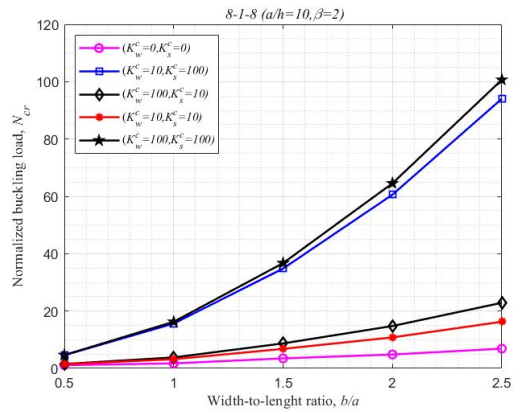
(a) $\beta = 0$ (b) $\beta = 10$

Figure 2. Relationship of the normalized buckling load N_{cr} and the length-to-thickness ratio a/h for different types of plate Type-B Al/ZnO$_2$ ($a/h = 10$)

(a) 1-8-1   (b) 8-1-8

Figure 3. Relationship of the normalized buckling load N_{cr} and the width-to-length ratio b/a for different types of plate Type-B Al/ZnO$_2$ ($a/h = 10$)

Table 3. Effect of the boundary conditions on the normalized buckling load N_{cr} for square plate $a/h = 10$ Type-B Al/ZnO$_2$ placed on an elastic base ($K_w^c = 10$, $K_s^c = 10$)

Boundary conditions	Gradient index β							
	0.0	0.5	1.0	2.0	5.0	6.0	8.0	10
CFFF	1.8252	1.8184	1.8157	1.8139	1.8129	1.8128	1.8127	1.8127
SFSF	2.3712	2.3482	2.3395	2.3334	2.3303	2.3301	2.3298	2.3296
SFSS	2.4168	2.3913	2.3815	2.3748	2.3714	2.3711	2.3708	2.3706
CCCF	3.6838	3.6181	3.5917	3.5717	3.5588	3.5574	3.5557	3.5546
SCSC	4.6985	4.6038	4.5654	4.5357	4.5154	4.5131	4.5101	4.5081

boundary conditions used at the plate borders regardless of the gradient index. In other words, the lowest and highest values of the normalized buckling load correspond to the CFFF and SCSC plates, respectively. Such behavior is due to the fact that higher constraints at the edges increase the plate flexural rigidity, leading to a higher normalized buckling load.

4. Conclusions

In this article, the buckling behavior of the FGSP laid on the elastic Pasternak foundation under in-plane compressive loads is analyzed. Both effects of the thickness stretching, and shear deformation are incoperated in the proposed RQ-3DTSDT integrated with the MKI meshless method. The variable unknowns of the present method is reduced to four resulting in considerably lower computation costs. The accuracy of the present method is justified by comparing the numerical results with the available ones. It can be concluded that the major parameters have considerable effects on the compressive buckling behaviors of the FG plates. The shear stiffness factor of the Pasternak-type foundation plays important role in increasing the normalized buckling load for the sandwich FG plates. The following major points can be drawn from the present study for the buckling behaviors of the symmetric FGSP with an FG core laid on the elastic foundations as follows:

- Increasing the gradient index leads to decreasing the normalized buckling load. The homogeneous ceramic plate has smaller values of normalized buckling loads than those of the corresponding FGSP.

- As the gradient index is less than unity, the increase of the skin layer thickness leads to a decrease significantly in normalized buckling load, and it is also clear that decreasing the plate-core thickness leads to decrease normalized buckling loads.

- As the gradient index is greater than, decreasing the skin layer thickness causes in decreasing the normalized buckling load, while increasing the core layer thickness leads to decreasing the normalized buckling loads.

- For FGSP plates with all boundary conditions on Pasternak support, the normalized buckling load is almost constant with respect to the variation of the gradient index.

Acknowledgement

References

[1] Love, A. E. H. (1888). The small free vibrations and deformation of a thin elastic shell. *Philosophical Transactions of the Royal Society of London*, 179:491–546.
[2] Mindlin, R. D. (1951). Influence of Rotatory Inertia and Shear on Flexural Motions of Isotropic, Elastic Plates. *Journal of Applied Mechanics*, 18(1):31–38.
[3] Reddy, J. N. (2006). *Theory and Analysis of Elastic Plates and Shells*. CRC Press.
[4] Lo, K. H., Christensen, R. M., Wu, E. M. (1977). A High-Order Theory of Plate Deformation—Part 2: Laminated Plates. *Journal of Applied Mechanics*, 44(4):669–676.
[5] Shimpi, R. P. (2002). Refined plate theory and its variants. *AIAA Journal*, 40:137–146.
[6] Carrera, E., Brischetto, S., Cinefra, M., Soave, M. (2011). Effects of thickness stretching in functionally graded plates and shells. *Composites Part B: Engineering*, 42(2):123–133.

[7] Murakami, H. (1986). Laminated Composite Plate Theory With Improved In-Plane Responses. *Journal of Applied Mechanics*, 53(3):661–666.

[8] Carrera, E. (1998). Mixed layer-wise models for multilayered plates analysis. *Composite Structures*, 43 (1):57–70.

[9] Carrera, E., Miglioretti, F., Petrolo, M. (2011). Accuracy of refined finite elements for laminated plate analysis. *Composite Structures*, 93(5):1311–1327.

[10] Talha, M., Singh, B. N. (2010). Static response and free vibration analysis of FGM plates using higher order shear deformation theory. *Applied Mathematical Modelling*, 34(12):3991–4011.

[11] Ganapathi, M., Makhecha, D. P. (2001). Free vibration analysis of multi-layered composite laminates based on an accurate higher-order theory. *Composites Part B: Engineering*, 32(6):535–543.

[12] Chen, C.-S., Hsu, C.-Y., Tzou, G. J. (2008). Vibration and Stability of Functionally Graded Plates Based on a Higher-order Deformation Theory. *Journal of Reinforced Plastics and Composites*, 28(10):1215–1234.

[13] Reddy, J. N. (2011). A general nonlinear third-order theory of functionally graded plates. *International Journal of Aerospace and Lightweight Structures (IJALS)*, 1(1).

[14] Ferreira, A. J. M., da Cunha Roque, C. M., Carrera, E., Cinefra, M., Polit, O. (2012). Analysis of sandwich plates by radial basis functions collocation, according to Murakami's Zig-Zag theory. *Journal of Sandwich Structures & Materials*, 14(5):505–524.

[15] Rodrigues, J., Roque, C., Ferreira, A., Cinefra, M., Carrera, E. (2012). Radial basis functions-differential quadrature collocation and a unified formulation for bending, vibration and buckling analysis of laminated plates, according to Murakami's Zig-Zag theory. *Computers & Structures*, 90-91:107–115.

[16] Maturi, D. A., Ferreira, A. J. M., Zenkour, A. M., Mashat, D. S. (2013). Analysis of Laminated Shells by Murakami's Zig-Zag Theory and Radial Basis Functions Collocation. *Journal of Applied Mathematics*, 2013:1–14.

[17] Neves, A., Ferreira, A., Carrera, E., Cinefra, M., Roque, C., Jorge, R., Soares, C. (2012). A quasi-3D hyperbolic shear deformation theory for the static and free vibration analysis of functionally graded plates. *Composite Structures*, 94(5):1814–1825.

[18] Neves, A. M. A., Ferreira, A. J. M., Carrera, E., Roque, C. M. C., Cinefra, M., Jorge, R. M. N., Soares, C. M. M. (2012). A quasi-3D sinusoidal shear deformation theory for the static and free vibration analysis of functionally graded plates. *Composites Part B: Engineering*, 43(2):711–725.

[19] Neves, A. M. A., Ferreira, A. J. M., Carrera, E., Cinefra, M., Roque, C. M. C., Jorge, R. M. N., Soares, C. M. M. (2013). Static, free vibration and buckling analysis of isotropic and sandwich functionally graded plates using a quasi-3D higher-order shear deformation theory and a meshless technique. *Composites Part B: Engineering*, 44(1):657–674.

[20] Zenkour, A. M. (2013). A simple four-unknown refined theory for bending analysis of functionally graded plates. *Applied Mathematical Modelling*, 37(20-21):9041–9051.

[21] Gu, L. (2002). Moving kriging interpolation and element-free Galerkin method. *International Journal for Numerical Methods in Engineering*, 56(1):1–11.

[22] Vu, T.-V., Curiel-Sosa, J. L., Bui, T. Q. (2018). A refined sin hyperbolic shear deformation theory for sandwich FG plates by enhanced meshfree with new correlation function. *International Journal of Mechanics and Materials in Design*, 15(3):647–669.

[23] Vu, T.-V., Nguyen-Van, H., Nguyen, C. H., Nguyen, T.-P., Curiel-Sosa, J. L. (2021). Meshfree analysis of functionally graded plates with a novel four-unknown arctangent exponential shear deformation theory. *Mechanics Based Design of Structures and Machines*, 1–33.

[24] Van, V. T., Tai, N. H. T., Hung, N. N. (2021). Static bending and free vibration analysis of functionally graded porous plates laid on elastic foundation using the meshless method. *Journal of Science and Technology in Civil Engineering (STCE) - NUCE*, 15(2):141–159.

[25] Reddy, J. N. (2005). *An introduction to the finite element method*. 3rd edition, McGraw-Hill New York.

[26] Akavci, S. S. (2016). Mechanical behavior of functionally graded sandwich plates on elastic foundation. *Composites Part B: Engineering*, 96:136–152.